ELSEVIER

Remote Sensing of Environment 79 (2002) 189–198

Remote Sensing of Environment

www.elsevier.com/locate/rse

Temperature and emissivity separation from multispectral thermal infrared observations

Thomas Schmugge[a,*], Andrew French[a], Jerry C. Ritchie[a], Albert Rango[a], Henk Pelgrum[b]

[a]USDA Agricultural Research Service Hydrology Laboratory, Building 007, BARC West, Beltsville, MD 20705, USA
[b]Earth Sciences Division, Keplerlaan I, 2201 AZ Noordwijk, Netherlands

Received 22 March 2000; received in revised form 3 October 2000; accepted 4 December 2000

Abstract

Knowledge of the surface emissivity is important for determining the radiation balance at the land surface. For heavily vegetated surfaces, there is little problem since the emissivity is relatively uniform and close to one. For arid lands with sparse vegetation, the problem is more difficult because the emissivity of the exposed soils and rocks is highly variable. With multispectral thermal infrared (TIR) observations, it is possible to estimate the spectral emissivity variation for these surfaces. We present data from the TIMS (Thermal Infrared Multispectral Scanner) instrument, which has six channels in the 8- to 12-μm region. TIMS is a prototype of the TIR portion of the ASTER (Advanced Spaceborne Thermal Emission and Reflection radiometer) instrument on NASA's Terra (EOS-AM1) platform launched in December 1999. The Temperature Emissivity Separation (TES) algorithm, developed for use with ASTER data, is used to extract the temperature and six emissivities from the six channels of TIMS data. The algorithm makes use of the empirical relation between the range of observed emissivities and their minimum value. This approach was applied to the TIMS data acquired over the USDA/ARS Jornada Experimental Range in New Mexico. The Jornada site is typical of a desert grassland where the main vegetation components are grass (black grama) and shrubs (primarily mesquite) in the degraded grassland. The data presented here are from flights at a range of altitudes from 800 to 5000 m, yielding a pixel resolution from 3 to 12 m. The resulting spectral emissivities are in qualitative agreement with laboratory measurements of the emissivity for the quartz rich soils of the site. The derived surface temperatures agree with ground measurements within the standard deviations of both sets of observations. The results for the 10.8- and 11.7-μm channels show limited variation of the emissivity values over the mesquite and grass sites indicating that split window approaches may be possible for conditions like these.

1. Introduction

Thermally emitted radiance from any surface depends on two factors: (1) the surface temperature, which is an indication of the equilibrium thermodynamic state resulting from the energy balance of the fluxes between the atmosphere, surface, and the subsurface soil; and (2) the surface emissivity, which is the efficiency of the surface for transmitting the radiant energy generated in the soil into the atmosphere. The latter depends on the composition, surface roughness, and physical parameters of the surface, e.g., moisture content. In addition, the emissivity generally will vary with wavelength for natural surfaces. Thus, to make a quantitative estimate of the surface temperature we need to separate the effects of temperature and emissivity in the observed radiation. An approach for doing this with multispectral thermal infrared (TIR) data will be presented and demonstrated with data acquired over the Jornada Experimental Range in New Mexico. This method has been successfully applied to TIMS data acquired over West Africa during the HAPEX-Sahel experiment (Schmugge, Hook, & Coll, 1998) but with little or no ground validation. In this paper, we have more supporting ground measurements of surface temperature to validate the approach. One of the objectives of these field experiments is to use the extracted surface temperature information in models to estimate the surface fluxes. In the future, we will be testing whether a two-source model that calculates the heat fluxes from the vegetation and soil separately can be used in these arid conditions with remotely sensed surface temperature information (Schmugge & Kustas, 1999; Schmugge, Kus-

* Corresponding author. Tel.: +1-301-504-8554; fax: +1-301-504-8931.
E-mail address: schmugge@hydrolab.arsusda.gov (T. Schmugge).

0034-4257/01/$ – see front matter
PII: S0034-4257(01)00272-3

tas, & Humes, 1998). An earlier application of the model in the more humid conditions of the Southern Great Plains experiment of 1997 (SGP97) is presented in the paper by French, Schmugge, and Kustas (2000a).

In addition to surface temperature observations these multispectral TIR data can be used to make estimates of the spectral variation of the surface emissivity. This information is important for the possible use of split window techniques in the TIR for estimating surface temperature directly from the multispectral measurements (Becker, 1987; Price, 1984; Wan & Dozier, 1996).

2. Methods and measurements

2.1. Thermal radiation

The intensity of the thermal radiation from an object is described by the Planck black body relationship given as a function of wavelength in Eq. (1):

$$L_{\mathrm{BB}}(\lambda, T) = \frac{2hc^2/\lambda^5}{\exp(hc/\lambda kT) - 1} \quad (1)$$

where h is the Planck's constant (6.626×10^{-34} J s), c is the speed of light (2.998×10^{8} m s^{-1}), k is the Boltzmann's constant (1.381×10^{-23} J K^{-1}), and L_{BB} is the spectral radiance (W m^{-2} sr^{-1} m^{-1}). At common terrestrial temperatures ($\sim$300 K), the peak emission occurs in the 8- to 10-μm range of wavelength. It is fortuitous that this peak occurs in a wavelength region where the atmosphere is relatively transparent compared to adjacent wavelengths. While the peak in atmospheric transmission is in the 8- to 12-μm range, there is still significant attenuation due primarily to water vapor. As a result, the magnitude of the atmospheric effect will depend on the water vapor content of the intervening atmosphere. This unknown or uncertain atmospheric contribution is one of the problems for the remote sensing of surface temperature at infrared wavelengths. This, of course, is in addition to clouds that will totally obscure the surface at visible and infrared wavelengths.

The radiances measured at the aircraft (A/C) are given by Eq. (2):

$$L_j(\mathrm{A/C}) = L_j(\mathrm{surf})\tau_j + L_j(\mathrm{atm}\uparrow) \quad (2)$$

where the values of the atmospheric transmission, τ_j, and upwelling radiation, $L_j(\mathrm{atm}\uparrow)$, can be calculated using the atmospheric radiative transfer model, MODTRAN (Berk et al., 1998), with atmospheric profile data measured at the nearby White Sands missile range. To obtain the values for the j-th channel on a multichannel instrument the output of MODTRAN is integrated over the spectral response function for that channel (see Fig. 1 for examples of the response

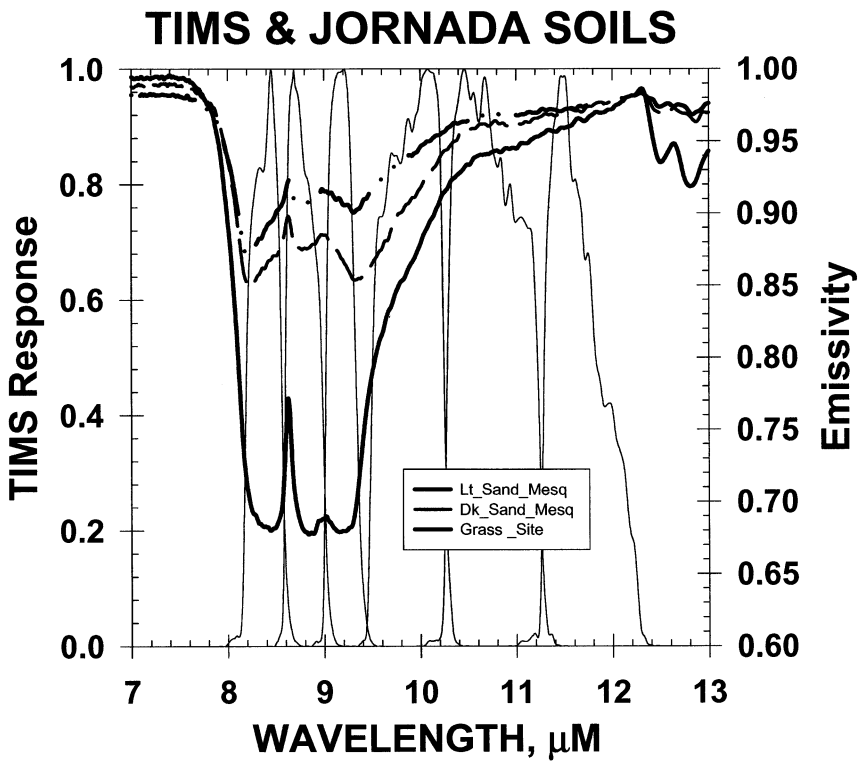

Fig. 1. Plots of the TIMS spectral response functions and laboratory measurements of the emissivity for the three soils from the Jornada. The TIMS channels are numbered 1–6 from the left. The upper emissivity curve is for soil from the grass site, the middle is for dark red soil from the mesquite site, and the bottom curve is for light sandy soil from the mesquite site.

functions). The values of τ_j and $L_j(\text{atm}\uparrow)$ were calculated as functions of angle, fitted to a secant relation, and used to obtain $L_j(\text{surf})$ on a pixel by pixel basis. This yields the upwelling radiance at the surface, which is given by:

$$L_j(\text{surf}) = \epsilon_j L_{\text{BB}}(\lambda_j, T_{\text{grd}}) + (1-\epsilon_j)L_j(\text{atm}\downarrow) \quad (3)$$

where $L_{\text{BB}}(\lambda,T)$ is the Planck equation for the radiation from a black body as given by Eq. (1) and λ_j is the central wavelength for the j-th channel. The value of $L_j(\text{atm}\downarrow)$ was determined by calculating the downwelling radiance as a function of angle and integrating over the hemisphere. The remaining problem is to relate these radiances to the surface emissivity in the six channels without direct knowledge of the temperature, T_{grd}.

2.2. Temperature/emissivity recovery

Eq. (3) indicates that if the radiance is measured in n spectral channels, there will be $n+1$ unknowns: the n emissivities and the surface temperature. Thus, additional information is needed to extract either the temperature or emissivity information. This has led to the development of a variety of techniques that differ according to the assumptions that they make. A review and analysis of some these approaches is given in the recent paper by Li, Becker, Stoll, and Wan (1999). The technique to be used here is the one used with data from the Advanced Spaceborne Thermal Emission Reflectance Radiometer (ASTER) on the Earth Observing System Platform, Terra (EOS-Terra), launched in December 1999 (Yamaguchi, Kahle, Tsu, Kawakami, & Pniel, 1998). This approach makes use of an empirical relation between the range of emissivities and the minimum value for a multichannel observations. It is termed Temperature Emissivity Separation or TES (Gillespie et al., 1998). The estimated kinetic temperature, T, is taken to be the maximum T estimated from the radiances for the n spectral channels calculated from Eq. (3) using an assumed emissivity value, ϵ (typically 0.98), so that surface types vegetation, snow, water, soil, and rock, will all be within ± 0.03 of the chosen value. Relative emissivities, β_j are found by ratioing the acquired radiance data (L_j), to the average of all channels (Eq. (4)):

$$\beta_j \equiv \frac{L_j/L_{\text{BB}}(\lambda_j, T)}{L/L_{\text{BB}}} \quad (4)$$

where the individual L_j are corrected for the effects of both the upwelling and downwelling atmospheric radiation. In principle, β_j may range widely, however, since the emissivities are generally restricted to 0.7–1.0, the ratioed values are restricted to 0.7–1.4. The β_j values provide a temperature independent index that can be matched against β_j values calculated from laboratory/field measurements of natural materials. In the TES method, the max − min difference ($\text{MMD} = \max(\beta_j) - \min(\beta_j)$) is related to the minimum emissivity. From laboratory measurements of emissivities (Salisbury & D'Aria, 1992), the relationship between $\epsilon_{\min}$ and MMD was found to be:

$$\epsilon_{\min} = 0.994 - 0.687 \times \text{MMD}^{0.737} \quad (5)$$

and can be used to calculate the emissivities from the β spectrum (Eq. (6)):

$$\epsilon_j = \beta_j \left(\frac{\epsilon_{\min}}{\min(\beta_j)} \right) \quad (6)$$

β_j is determined from the measured surface radiances L_j. From these ϵ_j a new temperature can be obtained. The process is repeated until the results converge and usually occurs after two or three iterations. A limitation of the method is that the smallest value of MMD is determined by instrument noise and the quality of atmospheric correction. This will affect the maximum ϵ that will be observed in the scene. This method has been successfully applied to TIMS data acquired over West Africa during the HAPEX-Sahel experiment (Schmugge, Hook & Coll, 1998). The sensitivity of TES to the atmospheric correction is discussed in a paper by Coll, Schmugge, and Hook (1998) using these same data.

2.3. TIMS

The data were obtained with the Thermal Infrared Multispectral Scanner (TIMS) sensor on board a DOE Cessna Citation aircraft on June 19 and September 30, 1997. TIMS has six channels in the TIR (8–12 μm) region of the electromagnetic spectrum. The instantaneous field of view is 2.5 mrad and the swath is ±40°. The spectral responses for the six channels are portrayed graphically in Fig. 1 along with laboratory measurements of the emissivity for three soils from the Jornada. It is clear that there is a variation of the emissivity over the six TIMS channels for these soils. The times and altitudes of the overflight are given in Table 1. Note that all the sites were covered by the high altitude pass.

As noted earlier, these A/C data were corrected for atmospheric effects using the MODTRAN path radiance model with atmospheric profiles appropriate for the conditions. For the June 19 flight, the profiles were obtained from the NOAA archive for the El Paso and Albuquerque stations and adjusted for the surface temperature and humidity conditions at the Jornada. For the September 30 flight, a sounding from the White Sands Missile range at

Table 1
Aircraft flight line times

Site	Date	Time (MST)	Altitude (m)	IFOV (m)
Grass	June 19, 1997	09:50	1500	4
Transition/mesquite		09:40	1500	4
High		10:15	5000	12
Grass	September 30, 1997	10:30	800	2
Transition/mesquite		10:45	800	2
High		11:02	5000	12

4AM MST was used. Again, the lower levels of the profile were adjusted to represent the surface conditions at the Jornada. The June profile was much drier with < 1 g/cm^2 of precipitable water while the September profile had 2.1 g/cm^2. However, for the 800-m altitude on that day only 0.5 g/cm^2 of water were below the aircraft.

2.3.1. The Jornada site

The Jornada Experimental Range lies between the Rio Grande flood plain (elevation 1190 m) on the west and the crest of the San Andres mountains (2830 m) on the east. The Jornada is 783 km^2 in area and is located 37 km north of Las Cruces, New Mexico on the Jornada del Muerto Plain in the northern part of the Chihuahuan Desert. A map showing the location of the range is given in Fig. 2. The larger Jornada del Muerto basin is typical of the Basin and Range physiographic province of the American Southwest and the Chihuahuan Desert (Havstad, Kustas, Rango, Ritchie, & Schmugge, 2000).

Three specific sites in the Jornada were chosen for intensive studies. Sites were selected to represent grass, shrub (mesquite), and grass–shrub transition areas. The grass site is in a fairly level area where black grama dominates and encompasses an exclosure where grazing has been excluded since 1969. Honey mesquite on coppice dunes dominates the shrub site. The dunes vary in height from 1 to 4 m with honey mesquite on each dune. Bare soil dominates the lower areas between these coppice dunes. The transition site has vegetation components from both the grass and shrub sites. We will present results from the grass and mesquite sites in this paper.

Vegetation surveys were performed in May 1997 and September 1997. These consisted of measurements along 150-m transects of the plant species and height and an estimate of LAI using the Licor LAI-2000. Along each transect, three 30-m segments were measured at 1-m intervals for a total of 90 measurements for each transect. For the grass and transitions sites, the LAI increased in September after the monsoon season with the biggest increased observed at the grass site (0.4 to 0.7); at the transition site, the increase was 0.6 to 0.7, and at the mesquite site, a decrease (0.9 to 0.7) was observed.

In support of the September 30, 1997 flight, ground measurements of surface temperature were made with a broadband handheld Everest Model 110 radiometer. The emissivity was set to 0.99, i.e., the observed radiance is converted to a temperature using this emissivity value. They have a 8–14-μm bandwidth and a 15° field of view, which translates to an area of about 20 cm in diameter when held 1 m above the surface. The measurements were made on a 7×7 grid with 5-m spacing at approximately the time of the aircraft overpass. Averages over these grids can be assumed

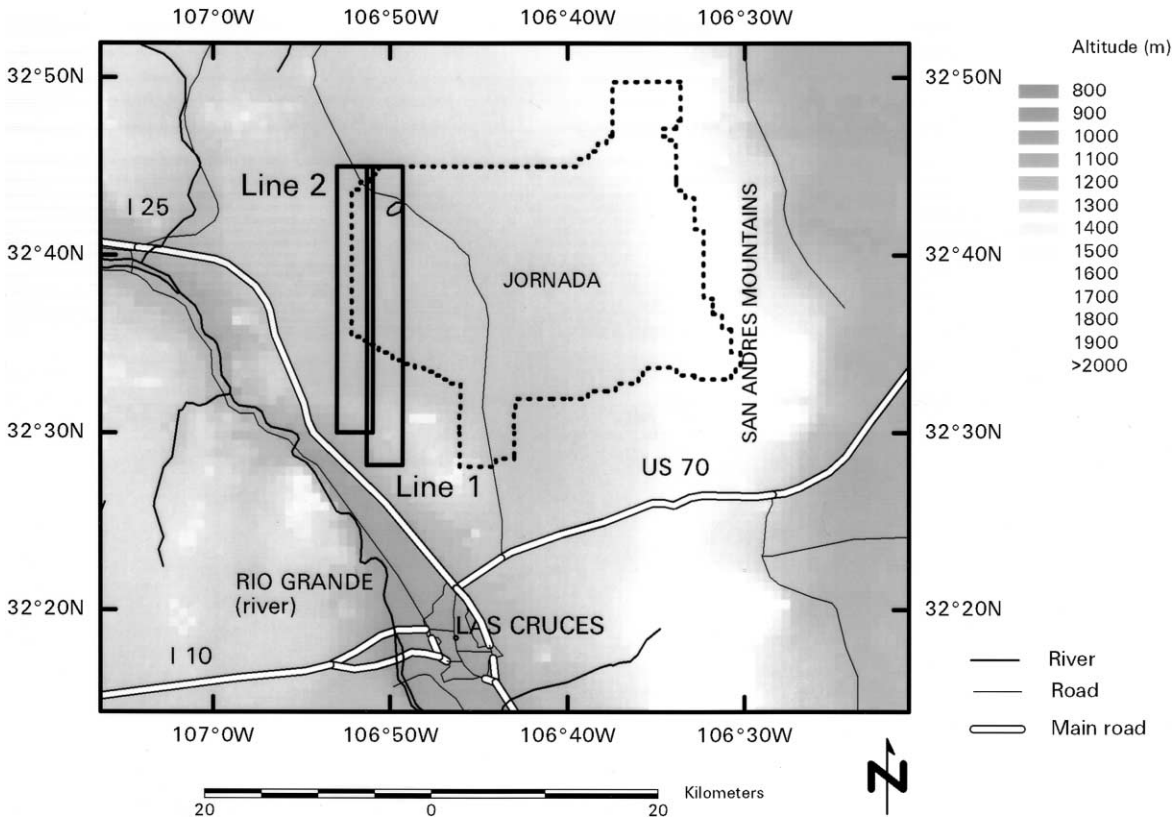

Fig. 2. The Jornada Experimental Range Site in New Mexico with topographical information is shown as shades of gray. The approximate areas covered by the two low level flight lines are shown. The grass site is covered by line 1, while the mesquite and transition sites are covered by line 2.

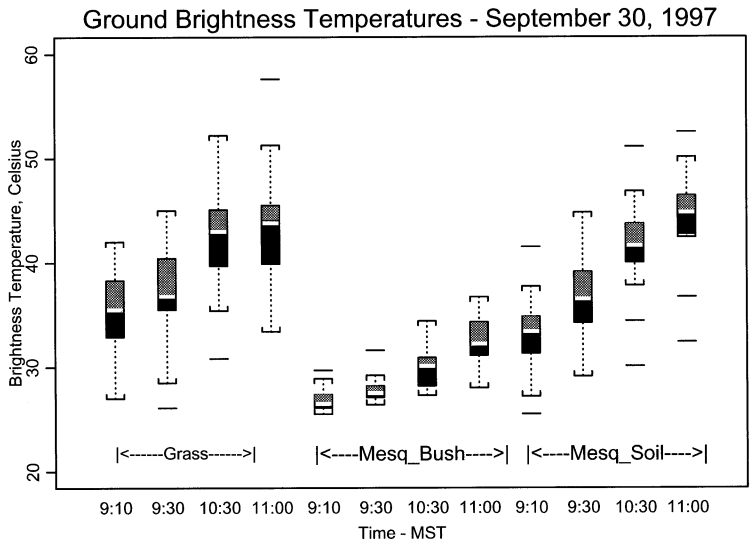

Fig. 3. Boxplots of IRT temperatures measured at the grass and mesquite site grids for four times on September 30, 1997. The box shows the range for half of the data in each case with the median value indicated by the open bar. The range of the data is shown by the capped brackets with outliers indicated by the lines outside the brackets.

to be representative of a 30×30-m area and will be compared with the A/C results.

A summary of the results from the grid measurements is presented in Fig. 3 as boxplots for the measurements at the two sites at the four times. The data from the mesquite site are split into bare and vegetated conditions. The measurements show the increase in temperature with time. Both the grass and bare soil results show more than 10°C variation over the grid with the grass measurements being only slightly cooler than the bare soil. This is because the grass at that time was mostly senescent. The 10:30 grid measurements bracket the aircraft overflight in time. In addition to the grid measurements, three Everest Model 4000 radiometers were used to continuously monitor the temperature evolution of three targets: a mesquite bush, a mixture of vegetation litter and bare soil. These radiometers also had a 15° IFOV and thus had about a 40-cm footprint on the target. These results are shown in Fig. 4. The bush temperature shows considerable short term variations due to wind fluctuations, ~ 2°C, which are not present in the litter or soil responses. The litter target with a mixture of dead vegetation and soil is probably similar to the average conditions on the

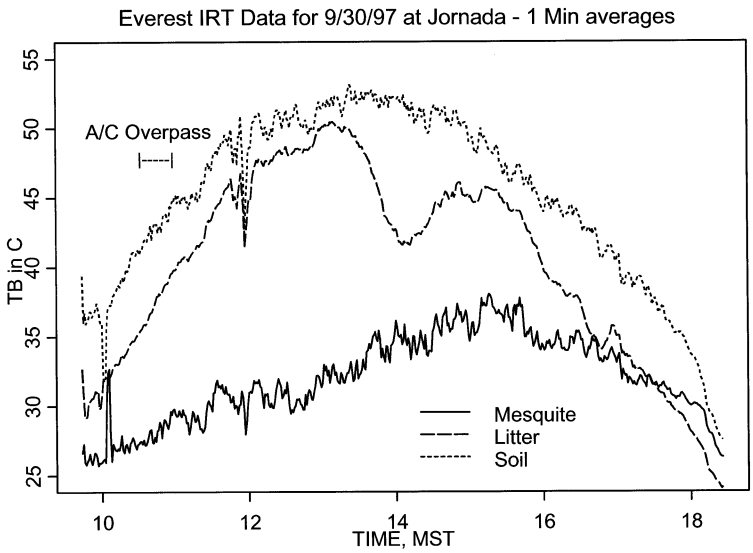

Fig. 4. Time evolution of IRT temperatures for the three targets at the Jornada on September 30, 1997. The spikes at 10:00 MST are due to a calibration blackbody being placed in front of each radiometer. The agreement was within a degree for each radiometer. The spike at 12:00 MST is probably due to a cloud shadow.

Table 2
Jornada soils' emissivities for the six TIMS channels and a broadband radiometer (BB)

	λ (μm)						
	BB	Channel 1	Channel 2	Channel 3	Channel 4	Channel 5	Channel 6
Soil/site	8–14	8.467	8.940	9.344	9.962	10.80	11.74
Transition	0.912	0.820	0.830	0.826	0.907	0.955	0.971
Light sand/mesquite	0.865	0.697	0.687	0.700	0.873	0.942	0.967
Dark sand/mesquite	0.930	0.871	0.879	0.863	0.914	0.961	0.973
Crust/grass	0.947	0.897	0.911	0.907	0.943	0.968	0.975

grass grid. The large decrease in the litter response at 14:00 MST is due to the shadow of bush cooling the target.

After a recent field experiment, soil samples from several of the sites in the Jornada were taken to the Jet Propulsion Laboratory for measurements of their emissivity spectra. The results for soils from the mesquite and grass site are shown in Fig. 1 along with the TIMS spectral response functions. The integrated values of the emissivity for each channel are given in Table 2 along with values for a typical 8–14-μm germanium window, which is typical for the Everest radiometers. From Table 2, we note that shortest wavelength channels, 1 and 2, have the largest variation (0.22) for the four samples, while the longest wavelength channel, 6, has an order of magnitude less variation (0.018). The calculated emissivities for a broadband radiometer typical of that used in our ground measurements is given for comparison.

3. Results and discussion

Fig. 5 presents a sample of the results from the September 30, 1997 flight. Images of Channel 1 (λ = 8.47 μm)

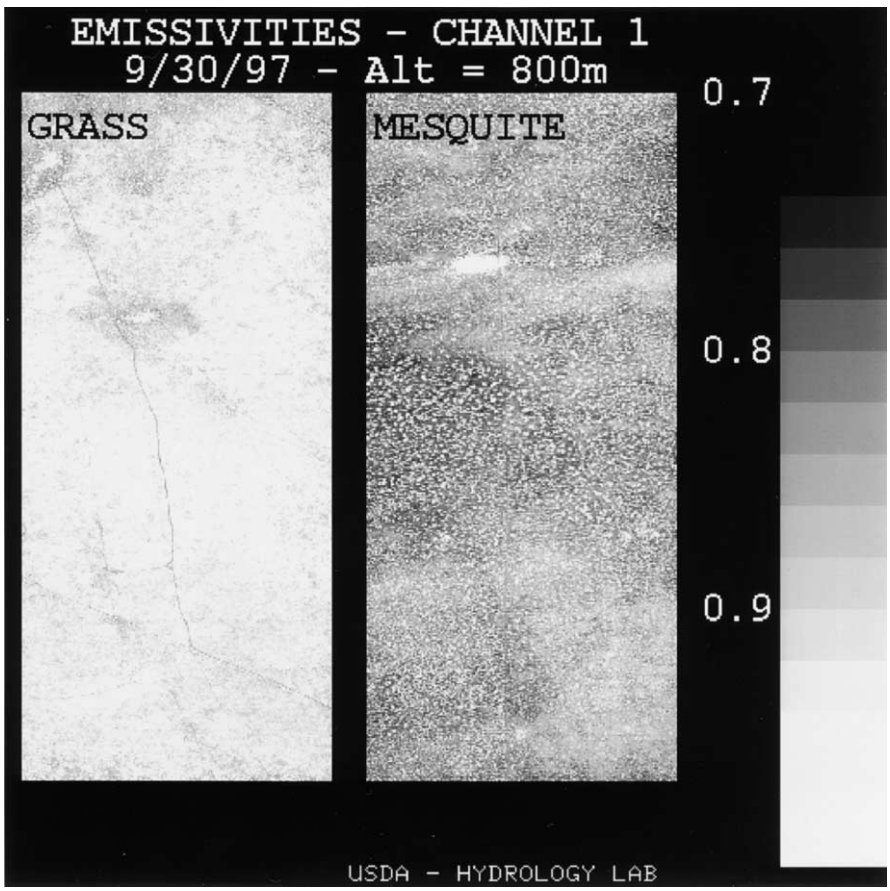

Fig. 5. Images of the Channel 1 (8.47 μm) emissivity for both the grass and mesquite sites using data acquired on September 30, 1997. North is up on these images, which are 2.7 km long and 0.9 km across.

emissivity are presented for the grass and mesquite sites. For the grass site the emissivity is relatively uniform except for the exposed soils along the roads and a couple of bare patches. The exclosure mentioned above is apparent to the left of the road in the middle of the image. The area inside the exclosure shows the most uniform and highest emissivities. The results for the mesquite site show almost the opposite results, i.e., mostly low emissivities due to the exposed soil between the mesquite dunes. The white spots are the mesquite bushes that have high emissivities. These results are quantified in Fig. 6, which presents histograms for each of the six channels at the two sites. For the grass site, the histogram is for an area within the exclosure, while for the mesquite it is for a much larger area covering the complete swath in the middle of the image. For the mesquite site, the short wavelength channels, 1–3, show a double peaked distribution indicative of pure soil pixels ($\epsilon \sim 0.8$), in reasonable agreement for a mixture of soils from the lab measurements, and a second smaller but sharper peak at $\epsilon \sim 0.98$, indicative of pure vegetation pixels. All six channels show this peak. For Channel 6, all the pixels are between 0.96 and 0.98, with a sharp cutoff at the lower end as expected because of the high emissivity for the soils at this wavelength. For the grass site, all six distributions are much

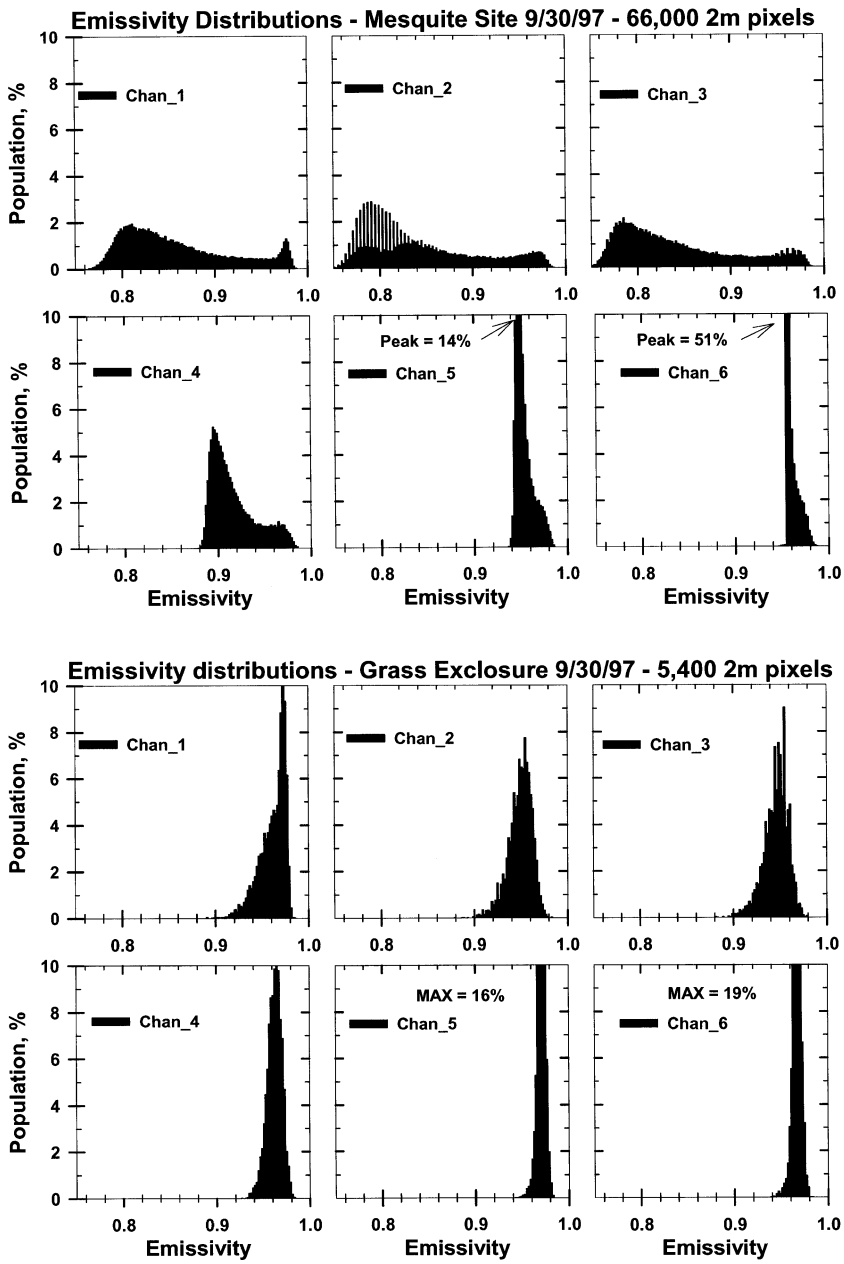

Fig. 6. Histograms of the emissivity distributions for the six TIMS channels for both the grass and mesquite sites on September 30, 1997.

tighter, with none of them showing the low emissivity behavior expected for pure soil pixels.

We also note that for both sites, there is little emissivity difference observed between Channel 5($\lambda = 10.8$ μm) and Channel 6($\lambda = 11.7$ μm), which is a positive sign for the use of split windows techniques to extract surface temperatures. The difference in lower edge for the two channels is ~ 0.02 for the mesquite site, which is comparable to that listed for the light sand soil from that site in Table 2. For the grass site, ϵ_5 is slightly greater than ϵ_6, with an average difference of 0.003.

The highest emissivities we observed were ~ 0.98 and the question is whether this is the true upper emissivity for these scenes or is it an artifact introduced by noise in the data, e.g., inaccurate atmospheric correction or differences in the calibration for the 6 channels. This noise would produce larger values of MMD for Eq. (5). We should note here that a similar analysis for a very heavy grass field at the El Reno Oklahoma Grazinglands Research site during the SGP97 found an average of 0.97 for heavily vegetated conditions (French, Schmugge, & Kustas, 2000b). So it would appear that TES is not able to extract high emissivity values ($\epsilon > 0.98$) from the observations.

The emissivity spectra obtained with the TIMS data for several sites are given in Fig. 7 along with some results from the lab measurements. The solid symbols are the TIMS spectra for a bare soil patch and a bush patch at the mesquite site and for a bare soil patch at the grass site. For comparison, results for three of the lab measurements are presented. The

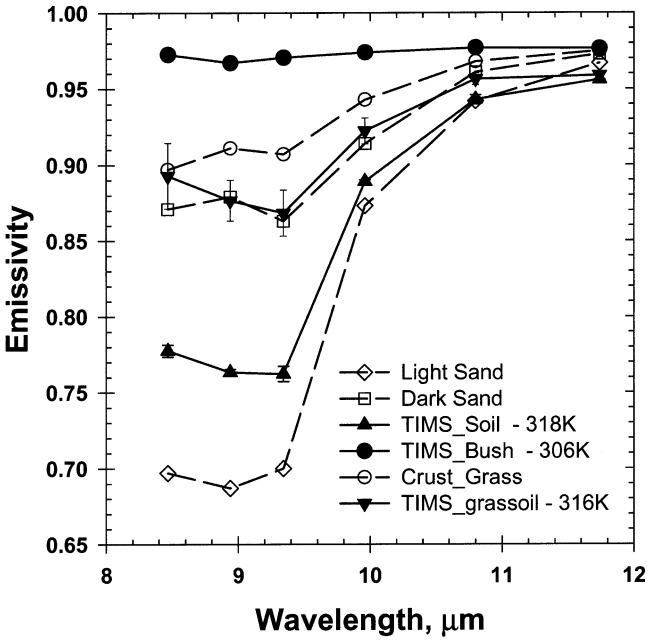

Fig. 7. Emissivity spectra derived from the TIMS data for bare soil and vegetation at the mesquite site and for a bare soil patch near the grass site. The solid lines with filled symbols are for the A/C results, the dashed lines with open symbols are for the laboratory measurements for soils from these sites.

Table 3
Ground–A/C comparisons of temperature

	Ground		A/C-TES	
Site	Samples	T (K)	Pixels	T (K)
Grass (grid)	49	315.7 ± 4.3	400	314.5 ± 1.2
Mesquite (bare)	21	314.8 ± 4.4	6	317.8 ± 0.7
Mesquite (vegetation)	9	303.3 ± 2.3	4	305.9 ± 2.1

bare soil at the mesquite site (solid triangles) shows a spectral behavior between that observed for the light and dark sands at that site indicating that a combination of the two soils is probably present in the patch sampled by TIMS. The soil at the grass site (inverted solid triangle) shows good agreement with the dark soil spectra but is a little lower than the results for the soil sample taken at the grass site, obtained near the exclosure. The TIMS patch was about 100 m to the north where there was about a 10 × 10-m apparent bare soil patch. The results from the vegetation (solid circles) show relatively little spectral variation as expected.

The A/C results for temperature are compared with the ground temperature measurements in Table 3 for a grid that was started at 10:30 MST, the measurements at each site took about 20 min. Thus, the aircraft overpass was at the beginning of the grid for the grass site and at the end of the grid for the mesquite site. These results indicate a reasonable agreement between the ground and A/C measurements especially when one considers that, e.g., for the bare soil, we sampled both the light and dark sand soils of Table 2. For the mesquite bush, the ground measurements were taken looking into the side of the bush, which is presumably cooler than the straight down view from the aircraft. For the bare soil case, recall that emissivity was taken into account for the A/C data but not for the ground measurements. If we assume that the TES results are a good approximation to the physical temperature, then the soil would need a broadband emissivity of about 0.95 to have the observed ground IRT temperature. In Table 2, the 8–14-μm emissivities for the light and dark sands were 0.865 and 0.93, respectively, for an average of about 0.9. However, an emissivity of 0.9 would imply that the downwelling atmospheric radiation could have a significant effect toward bringing them into agreement.

As noted earlier, there was an overflight on June 19, 1997 at the 1500-m altitude, which produced coverage at 4-m resolution. The histograms of the emissivity distributions for this flight are presented in Fig. 8. The distributions are very similar to those from the September 30 flight with a couple of small differences. The vegetation peaks at the mesquite site are not apparent in the data for the first three channels. This, perhaps, is due to the coarser resolution and the drier conditions. The emissivity of the shorter wavelength channels (1–3) on June 19, 1997, at the grass site are lower, which we believe is due to poorer vegetation conditions on that date as indicated by the LAI reading noted earlier for the grass site. The basic distributions of the emissivity for both sites are essentially the same for the

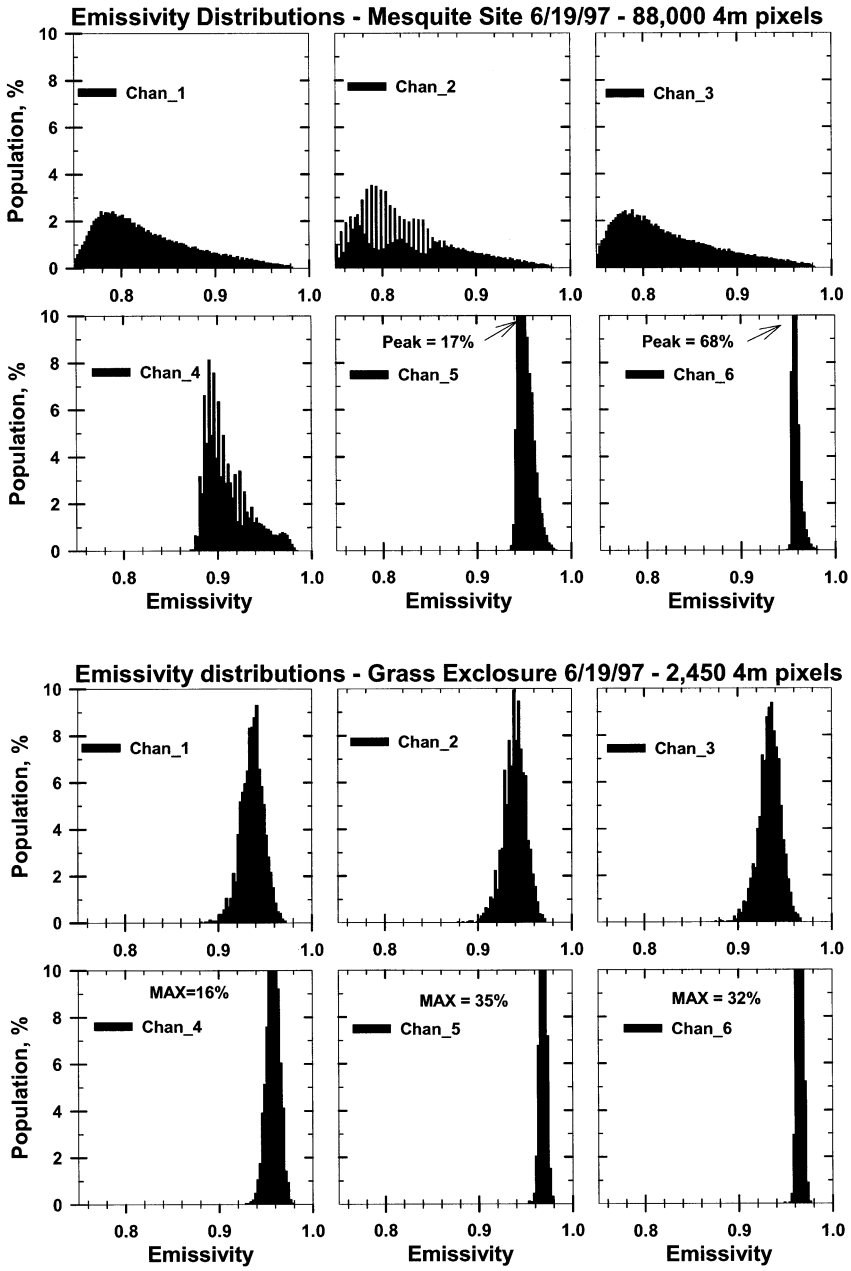

Fig. 8. Histograms of the emissivity distributions for the six TIMS channels for both the grass and mesquite sites on June 19, 1997.

2 days, which is an indication of the robustness of the TES approach.

4. Conclusions

Remotely sensed multispectral TIR observations over an arid landscape were analyzed to extract values of the surface temperature and spectral emissivity. The results were compared with ground and laboratory measurements and found to be in reasonable agreement. The spectral emissivity results were in good agreement with the laboratory measurements of the emissivity for typical soils from the area when one considers that the remotely sensed data are averaged over the different soils within the sensor's field of view. The derived temperatures were in good agreement with surface IRT measurements for both vegetation and bare soil. The agreement of results from the flights 2 months apart at different resolutions is also a positive indication that the TES algorithm is working well. The results for the 10.8- and 11.7-μm channels show limited spatial variation of the emissivity values over both the mesquite and grass sites indicating that split window approaches may be possible for conditions like these quantifying the differences in emissivity for these two channels is limited by the noise in the system. This also limits the ability of TES and multispectral

TIR observations to determine ϵ for high emissivity targets. With these caveats, we believe that the results presented here indicate that it will be possible to use the TES algorithm with multispectral TIR data from the ASTER instrument on the EOS-Terra spacecraft to obtain large scale maps of the surface emissivity and its spectral variation.

Acknowledgments

This research was supported by the ASTER Project of NASA's EOS-Terra Program. The laboratory emissivity measurements were made by Cindy Grove of the Jet Propulsion Laboratory. We want to thank the Met Branch of the White Sands Missile range for making their radiosoundings available.

References

Becker, F. (1987). The impact of spectral emissivity on the measurements of land surface temperature from a satellite. *International Journal of Remote Sensing*, *8*, 1509–1522.

Berk, A., Bernstein, L. S., Anderson, G. P., Acharya, P. K., Robertson, D. C., Chetwynd, J. H., & Adler-Golden, S. M. (1998). MODTRAN cloud and multiple scattering upgrade with application to AVIRIS. *Remote Sensing of Environment*, *65*, 367–375.

Coll, C., Schmugge, T. J., & Hook, S. J. (1998, September). Atmospheric effects on the Temperature Emissivity Separation algorithm. *Proceedings of the SPIE (Barcelona)*, *3499*, 405–415.

French, A. N., Schmugge, T. J., & Kustas, W. P. (2000a). Estimating surface fluxes over the SGP site with remotely sensed data. *Physics and Chemistry of the Earth*, *25* (2), 167–172.

French, A. N., Schmugge, T. J., & Kustas, W. P. (2000b). Discrimination of senescent vegetation using thermal emissivity contrast. *Remote Sensing of Environment*, *74*, 249–254.

Gillespie, A., Rokugawa, S., Matsunaga, T., Cothern, J. S., Hook, S., & Kahle, A. B. (1998). A temperature and emissivity separation algorithm for Advanced Spaceborne Thermal Emission and Reflection radiometer (ASTER) images. *IEEE Transactions on Geoscience and Remote Sensing*, *36*, 1113–1126.

Havstad, K. M., Kustas, W. P., Rango, A., Ritchie, J., & Schmugge, T. J. (2000). Jornada experimental range: a unique location for remote sensing experiments to validate EOS satellite systems and to understand the effects of climate change in arid environments. *Remote Sensing of Environment*, *74* (1), 13–23.

Li, Z. L., Becker, F., Stoll, M. P., & Wan, Z. M. (1999). Evaluation of six methods for extracting relative emissivity spectra from thermal infrared images. *Remote Sensing of Environment*, *69*, 197–214.

Price, J. C. (1984). Land surface temperature measurements from the split window bands of the NOAA 7 advanced very high resolutions radiometer. *Journal of Geophysical Research*, *89*, 7231–7237.

Salisbury, J. W., & D'Aria, D. M. (1992). Emissivity of terrestrial materials in the 8–14 mm atmospheric window. *Remote Sensing of Environment*, *42*, 83–106.

Schmugge, T., Hook, S. J., & Coll, C. (1998). Recovering surface temperature and emissivity from thermal infrared multispectral data. *Remote Sensing of Environment*, *65*, 121–131.

Schmugge, T. J., & Kustas, W. P. (1999). Radiometry at infrared wavelengths for agricultural applications. *Agronomie*, *19*, 83–96.

Schmugge, T. J., Kustas, W. P., & Humes, K. S. (1998). Monitoring of land surface fluxes using ASTER observations. *IEEE Transactions on Geoscience and Remote Sensing*, *36*, 1421–1430.

Wan, Z., & Dozier, J. A. (1996). Generalized split-window algorithm for retrieving land-surface temperature for space. *IEEE Transactions on Geoscience and Remote Sensing*, *34*, 892–905.

Yamaguchi, Y., Kahle, A. B., Tsu, H., Kawakami, T., & Pniel, M. (1998). Overview of Advanced Spaceborne Thermal Emission and Reflection radiometer (ASTER). *IEEE Transactions on Geoscience and Remote Sensing*, *36*, 1062–1071.